

**A 3-D wavelet analysis of substructure in the Coma cluster:
statistics and morphology**

M. Gambera

Istituto di Astronomia, Università di Catania, Italy

A. Pagliaro

Istituto di Astronomia, Università di Catania, Italy

V. Antonuccio-Delogu¹

Osservatorio Astrofisico di Catania, Italy

and

U. Becciani

Osservatorio Astrofisico di Catania, Italy

Received _____; accepted _____

submitted to Ap.J.

¹Also: Theoretical Astrophysics Center, Copenhagen, Denmark

ABSTRACT

Evidence for clustering within the Coma cluster is found by means of a multiscale analysis of the combined angular-redshift distribution. We have compiled a catalogue of 798 galaxy redshifts from published surveys from the region of the Coma cluster. We examine the presence of substructure and of voids at different scales ranging from ~ 1 to $\sim 16 h^{-1}$ Mpc, using subsamples of the catalogue, ranging from $cz = 3000$ km/s to $cz = 28000$ km/s. Our substructure detection method is based on the wavelet transform and on the segmentation analysis. The wavelet transform allows us to find out structures at different scales and the segmentation method allows us a quantitative statistical and morphological analysis of the sample. From the whole catalogue we select a subset of 320 galaxies, with redshifts between $cz = 5858$ km/s and $cz = 8168$ km/s that we identify as belonging to the central region of Coma and on which we have performed a deeper analysis, on scales ranging from $180 h^{-1}$ kpc to $1.44 h^{-1}$ Mpc. Our results are expressed in terms of the number of structures or voids and their sphericity for different values of the threshold detection and at all the scales investigated. According to our analysis, there is strong evidence for multiple hierarchical substructure, on scales ranging from a few hundreds of kpc to about $4 h^{-1}$ Mpc. The morphology of these substructures is rather spherical. On the scale of $720 h^{-1}$ kpc we find two main subclusters which were also found before, but our wavelet analysis shows even more substructures, whose redshift position is approximately marked by these bright galaxies: NGC 4934 & 4840, 4889, 4898 & 4864, 4874 & 4839, 4927, 4875.

Subject headings: galaxies: clusters: general - galaxies: clusters: individual (Coma) - galaxies: structure - method: data analysis

1. Introduction

The Coma cluster (number 1656 in the Abell [1958] catalogue) has been perhaps the most studied galaxy cluster since 1933, when Zwicky calculated its mass (Zwicky, 1933). It has been long quoted as the paradigmatic example of a roughly spherical, relaxed cluster (Sarazin, 1986). Previous papers (e.g. Fitchett & Webster, 1987; Mellier et al., 1988; Baier et al., 1990; Briel et al., 1992; White et al., 1993; Colless & Dunn, 1996, hereafter CD96 and Biviano et al., 1996) have suggested that this cluster may have a complex structure. The X-ray images obtained with *ROSAT* suggest the presence of clumps of emission associated with substructures (Briel et al., 1992; White et al., 1993). However, previous analysis were performed only on 2-D slices of the cluster. In this paper we take up the issue of substructure in this cluster by yet another point of view, namely by trying to make use of redshift information.

Our aim is to find out substructure or voids at different scales through a three-dimensional analysis of the cluster, identify them and make a morphological analysis. As it will be evident, our wavelet analysis detects substructure which is not visible in 2-D images, either optical and/or X-ray.

The plan of the paper is as follows: in §2 we discuss which selection criteria we have adopted to assemble our catalogue. In §3 and in §4 we discuss the method of analysis based on wavelet transform and segmentation. In §5 we report our results concerning the number and morphology of substructures and in §6 we do the same for the central region of the cluster. In §7 we make some cautionary remarks concerning the statistical and physical significance of our analysis, and finally in §8 we report our conclusions.

2. The Data

A large body of data on the Coma cluster is available in the literature. The catalogue has been collected exploiting data coming from different redshift surveys. In total we have selected 798 redshift for galaxies lying in the range:

$$\begin{aligned} RA &= 10^h 42^m 00^s, 15^h 28^m 00^s \\ DEC &= +26^\circ 30' 00'', +29^\circ 55' 00'' \end{aligned} \tag{1}$$

(B1950.0, hereafter all coordinates are referred to 1950.0). The redshifts for 243 galaxies have been kindly provided to us in electronic form by J. Colless and come from the new redshifts survey by CD96. The mean redshift uncertainty is: of about 50 km/s, and the uncertainty in the positions is less than 1". Another sample of 305 redshifts have been taken from Biviano et al. (1996); 225 of them are new measurements made at the Canada-France-Hawaii Telescope; the mean uncertainty is about 100 km/s. The positions in this catalogue are known with a mean error of about 2". Another 320 redshifts have been taken from the catalogue of 379 galaxies by I. D. Karachentsev & A. I. Kopylov (1990). The mean uncertainty in their measurements is 100 km/s, while the mean error in the positions is $\pm 3''$. Finally, another 46 redshifts have been taken from the NED (NASA Extragalactic Database). This latter set of data is heterogeneous, however their quoted mean uncertainty is less than ~ 120 km/s whilst the position are known with a mean error of about 6".

The total number of galaxies so collected is 914, but some objects are common to the three data sets. We have considered a galaxy common when its position in a given data set is inside the mean error in the coordinate determination of a different set. So, if for the same galaxy several redshift measurements were available, we have included only the most accurate one.

| | # gal | $\langle cz \rangle$ | σ_{cz} | $(cz)_{min}$ | $(cz)_{max}$ |
|-----------|-------|----------------------|---------------|--------------|--------------|
| C_{ext} | 690 | 10541 ± 115 | 6056 ± 98 | 3000 | 28000 |
| C | 485 | 7013 ± 100 | 1155 ± 80 | 4000 | 10000 |
| C_{cen} | 320 | 7034 ± 80 | 597 ± 70 | 5855 | 8168 |

Table 1: Catalogs used in our analysis. Redshifts are in km/s

The completeness of our heterogeneous catalogue is about 85% at $m_B = 18$. This value has been calculated from a weighted mean of the values for the different database used in our compilation.

To summarize, we have a heterogeneous sample of redshifts for 798 galaxies with $1000 \leq cz \leq 115000$ km/s. As coordinates for cluster’s photometric centre we choose the value quoted by Godwin et al. (1983): RA = $12^h57^m.3$ and DEC = $+28^\circ14.4'$. The uncertainty on the redshifts measurement is about 100 km/s and the maximum error on the positions is less than $3''$. From this catalogue we extract three different subsamples as shown in Table 1. The line-of-sight distribution for the galaxies of our subsample with $3000 \text{ km/s} < cz < 28000 \text{ km/s}$ is shown in fig. 1a. Hereafter we call this region C_{ext} . The number of galaxies inside this region is 690. already this histogram seems to suggest the presence of two main peaks in the redshift distribution.

The subsample C_{ext} has a mean redshift $\langle cz \rangle = (10541 \pm 115)$ km/s and a standard deviation $\sigma_{cz} = (6056 \pm 98)$ km/s. The galaxies of the first peak have redshifts $4000 \leq cz \leq 10000$ km/s; the mean redshift and the standard deviation being respectively $\langle cz \rangle = (7013 \pm 100)$ km/s and $\sigma_{cz} = (1155 \pm 80)$ km/s. The line-of-sight velocity dispersion for the galaxies of the first peak is $\sigma_v = (1128 \pm 78)$ km/s. The galaxies of the second peak have redshifts $16100 \leq cz \leq 24600$ km/s, mean redshift and standard deviation being respectively $\langle cz \rangle = (19918 \pm 100)$ km/s and $\sigma_{cz} = (3745 \pm 80)$ km/s. In Fig. 1b only those galaxies inside the first peak are considered and the line-of-sight distribution is shown.

Hereafter we call this region C . The number of galaxies inside C is 485. From Fig. 1b we note that the distribution of Coma galaxies in the redshift field show the presence of some peaks and this also may suggest the existence of multiple substructure.

We have transformed the angular distances from the photometric center to linear one assuming a distance from the center of the cluster equal to the mean value of the redshift divided by H_0 . Finally, to make our linear coordinates independent from the value of H_0 , we renormalize them dividing by σ_{cz} .

3. The method of analysis: wavelet transform and segmentation.

3.1. The wavelet transform

Our method of structure detection is based on the wavelet transform evaluated at several scales and on the segmentation analysis, and is similar to the one developed by Lega (1994, hereafter L94; part of this Ph.D. thesis may be found in Lega et al., 1995).

A detailed description of the implementation of the algorithms is beyond the purpose of this paper. A parallel version for a Connection Machine *CM200* has been developed by Lega (L94), a new *PVM* version will be described in Pagliaro & Becciani (1997). Although the method we implement is three-dimensional for simplicity we describe here the one dimensional version: the generalization to the 3-D case is straightforward.

For a one-dimensional function $f(x)$ the wavelet transform is a linear operator that can be written as:

$$\begin{aligned} w(s, t) &= \langle f | \psi \rangle \\ &= s^{-1/2} \int_{-\infty}^{+\infty} f(x) \psi^* \left(\frac{x-t}{s} \right) dx \end{aligned} \quad (2)$$

where $s(> 0)$ is the scale on which the analysis is performed, $t \in \Re$ is the spatial translation

parameter and ψ is the the Grossmann-Morlet (1984, 1987) analyzing wavelet function

$$\psi_{(s,t)}(x) = s^{-1/2}\psi\left(\frac{x-t}{s}\right) \quad (3)$$

that is spatially centered around t and has scale s . The wavelet function $\psi_{(1,0)}(x)$ is called *mother wavelet*. It generates the other wavelet function $\psi_{(s,t)}(x)$, $s > 1$. We follow L94 in the choice of the mother wavelet:

$$\psi_{(s,t)}(x) = \phi(x) - \frac{1}{2}\phi\left(\frac{x}{2}\right) \quad (4)$$

where ϕ is the cubic centred B-spline function defined by:

$$\phi(x) = \frac{|x-2|^3 - 4|x-1|^3 + 6|x|^3 - 4|x+1|^3 + |x+2|^3}{12} \quad (5)$$

Although our data distribution is highly anisotropic, we prefer to use an isotropic wavelet function and to perform a scale transformation along the z (redshift) axis.

With these choices, the wavelet coefficients at different scales can be calculated by the *à trous* algorithm, as described by L94 (pag.100), which is extremely fast and requires the set of scales to be powers of two: $s = 2^r$.

The scale s in this kind of analysis may be considered the resolution. In other words, if we perform a calculation on a scale s_0 , we expect the wavelet transform to be sensitive to structures with typical size of about s_0 and to find out those structures.

3.2. Choice of threshold

The thresholding is made on the wavelet coefficient histogram. For a flat background, the wavelet transform yields zero coefficients. The existence of structures at a given scale gives wavelet coefficient with large positive values. Obviously, a random distribution may result in coefficients different even if there is no structure, due to statistical fluctuations.

Moreover, the statistical behaviour of the wavelet coefficient is complex because of the existence of correlation among nearby background structures which reflect in correlations among nearby pixels.

In order to single out significant structures we have to fix a tresholding criterion and level. We choose the threshold using a classical decision rule. We calculate the wavelet coefficients $w_{ran}(s)$ for each scale of our analysis, for 10 random distribution in the same region of space of our data and on the same grid. Then we calculate the probability $P[w(s) \leq w_{ran}(s)]$ and choose the value $w_{thres}(s)$ so that:

$$P[w_{thres}(s) \leq w_{ran}(s)] \leq \epsilon \tag{6}$$

Our threshold on the scale s is the value $\nu_{thres} = w_{thres}(s)$. Our choice for the value of ϵ is:

$$\epsilon = 0.001 \tag{7}$$

that ensures a 99.9% confidence level in the structure detection.

However, for the sake of completeness, we perform our analysis for several values of the threshold, calculated in terms of the standard deviation in the wavelet coefficient distribution of our data.

3.3. Structure numbering through segmentation

The second step of our analysis is the determination of connected pixels over a fixed threshold (*segmentation*, Rosenfeld 1969), the numbering of the selected structures and their morphological analysis.

The segmentation and numbering consists of the analysis of the wavelet coefficients' matrix; all the pixels associated with a wavelet coefficient greater than the selected threshold are labeled with an integer number. All other pixels labels are set equal to zero.

Then, the same label is associated with all the pixels connected in a single structure, in a sequential way. So, the first structure individuated has the label '1' and so on. Then, for each structure we calculate volume and surface and from them a morphological parameter.

The detailed description of the algorithm is beyond the purpose of this paper. However it can be described in brief as follows: *Step 1*: all pixels with $w \geq \nu_{thres}$ are labeled. *Step 2*: the same label is associated with those pixels labeled and connected. This is done in a sequential way: the first structure detected has the label '1', the N -th one has the label 'N'. This requires a renumbering of most pixels. *Step 3*: volume and surface of each structure singled out are calculated.

3.4. The morphological parameter

In order to perform a morphological analysis we have to introduce a morphological parameter that quantifies the sphericity of the structures. We choose the parameter:

$$L(s) = K(s) \frac{V^2}{S^3} \quad (8)$$

where V is the volume and S is the surface, as in L94, and $K(s)$ is a parameter that depends on the scale of analysis. We want $L(s)$ to have the following behaviour: zero for very filamentary structures and 1 for spherical ones. This may be achieved putting $K = 36\pi$, but only for those scales not affected by the granular nature of the analysis. We choose the value 36π only for the scales $s = 2^r$ pixels with $r \geq 2$. For the smallest scales the constant 36π is not adequate, since we are close to the grid resolution and the geometry of the substructures cannot be spherical. So, since we want to consider as spherical a one-pixel structure, we adopt the values:

$$K(2^r) = \begin{cases} 216 & \text{if } r = 0, 1 \\ 36\pi & \text{otherwise} \end{cases} \quad (9)$$

Then, for every detection threshold we calculate the values:

$$\langle L(s) \rangle = \sum_{i=1}^{N_{obj}} \frac{L(s)}{N_{obj}} \quad (10)$$

where N_{obj} is the number of objects detected at scale s .

4. The voids detection method

Voids detection method is analogue to structure detection method, as far as "greater than" is replaced by "less than". The voids thresholding is made on the wavelet coefficient histogram too. The presence of voids at a given scale gives wavelet coefficient with large negative values.

Our choice for the threshold is the same as in §3.2. We calculate the wavelet coefficients $w_{ran}(s)$ for each scale of our analysis, for 10 random distribution in the same region of space of our data. Then we calculate the probability $P[w(s) \geq w_{ran}(s)]$ and choose the value $w_{voids}(s)$ so that:

$$P[w_{voids}(s) \geq w_{ran}(s)] \leq \epsilon \quad (11)$$

with $\epsilon = 0.001$, that ensures a 99.9% confidence level in the voids detection. Our threshold is the value $\nu_{voids} = w_{voids}(s)$. Obviously, in the segmentation algorithm for the voids detection the labeled pixels are those with the wavelet coefficients: $w \leq \nu_{voids}$.

The determination of the voids' morphological parameter values is analogue to the determination of structures' morphological parameter value as described in §3.4.

5. Substructure and voids detection in the Coma cluster

We examine two catalogues. The first is C_{ext} made of 690 galaxies, as previously said, with redshifts between $cz = 3000$ km/s and $cz = 28000$ km/s. Our grid ensures a resolution

of about $2 h^{-1}$ Mpc on each of the three axis. We examine four different scales: 2.02, 4.04, 8.08, $16.16 h^{-1}$ Mpc, for four different values of the threshold: the 99.9% confidence level as described in §3, and then: 3σ , 4σ and 5σ , where σ is the standard deviation in the wavelet coefficient distribution for the selected scale. The second catalogue investigated is C . It is made of 485 galaxies with redshifts between $cz = 4000$ km/s and $cz = 10000$ km/s. Our analysis grid ensures a resolution of about $470 h^{-1}$ kpc on each of the three axis. We examine four different scales: 0.47, 0.94, 1.88, $3.76 h^{-1}$ Mpc, for the same four different values of the threshold as before. We show the wavelet coefficients distributions on the four scales for the two catalogues in Fig.2÷3. We plot the value $(w - \langle w \rangle)/\sigma$, where w is the wavelet coefficient value and $\langle w \rangle$ and σ are the mean and the standard deviation in the wavelet coefficient distribution, versus $\text{Log}_{10}P(w)$, where $P(w)$ is the probability associated to the wavelet coefficient w .

| 1. structures | | | | | | 2. morphology | | | | | |
|---------------|-------|-----------|-----------|-----------|-------|---------------|-------|-----------|-----------|-----------|-------|
| scale | 99.9% | 3σ | 4σ | 5σ | voids | scale | 99.9% | 3σ | 4σ | 5σ | voids |
| 2.02 | 60 | 63 | 55 | 64 | 65 | 2.02 | 0.93 | 0.90 | 0.91 | 0.91 | 0.84 |
| 4.04 | 15 | 4 | 4 | 4 | 2 | 4.04 | 0.52 | 0.40 | 0.45 | 0.27 | 0.13 |
| 8.08 | 2 | 1 | 1 | 1 | 4 | 8.08 | 0.30 | 0.27 | 0.27 | 0.31 | 0.42 |
| 16.16 | 2 | 1 | 2 | 2 | 0 | 16.16 | 0.17 | 0.17 | 0.30 | 0.31 | - |

Table 2: Number of structures and mean morphological parameter $\langle L \rangle$ at different scales and over different thresholds for the catalog C_{ext} . Scales are expressed in Mpc.

The curves are slightly asymmetric on all the scales, with a small queue towards the positive values of the coefficients, meaning presence of substructure. Our results are expressed in terms of number of structures at the selected scales (see the Tables 2 and 3). Considering the 99.9% confidence level as a significance level for the structure detection, we have overwhelming evidence for substructure inside the Coma cluster on scales from 0.47

to $4.04 h^{-1}$ Mpc. On smaller scales the evidence is certainly lesser, as one can also see from the fact that on these scales the wavelet coefficients’ histograms are more symmetric.

In Tables 2 and 3 we show the morphological parameter $\langle L \rangle$. For what concerns C , our substructures are rather spherical on the first two scales. The value of $\langle L \rangle$ is lowered till 0.2 on the scale $1.88 h^{-1}$ Mpc, meaning a much more filamentary morphology for those structures singled out at this resolution. The substructure of C_{ext} , singled out with a greater resolution shows a spherical morphology till the scale of $2.02 h^{-1}$ Mpc; more elongated shapes are found out at the bigger scales. In both cases the diminution of $\langle L \rangle$ and of the number of structures as a function of the scale indicates a hierarchical distribution.

| 1. structures | | | | | | 2. morphology | | | | | |
|---------------|-------|-----------|-----------|-----------|-------|---------------|-------|-----------|-----------|-----------|-------|
| scale | 99.9% | 3σ | 4σ | 5σ | voids | scale | 99.9% | 3σ | 4σ | 5σ | voids |
| 2.02 | 60 | 63 | 55 | 64 | 65 | 2.02 | 0.93 | 0.90 | 0.91 | 0.91 | 0.84 |
| 4.04 | 15 | 4 | 4 | 4 | 2 | 4.04 | 0.52 | 0.40 | 0.45 | 0.27 | 0.13 |
| 8.08 | 2 | 1 | 1 | 1 | 4 | 8.08 | 0.30 | 0.27 | 0.27 | 0.31 | 0.42 |
| 16.16 | 2 | 1 | 2 | 2 | 0 | 16.16 | 0.17 | 0.17 | 0.30 | 0.31 | - |

Table 3: Number of structures and mean morphological parameter $\langle L \rangle$ at different scales and over different thresholds for the catalog C_{ext} . Scales are expressed in h^{-1} Mpc.

6. The central region of Coma

6.1. Substructures

We consider a galaxy belonging to the central region of Coma if its redshift is inside $\pm 1\sigma$ from $\langle cz \rangle = 7013$ km/s, where $\langle cz \rangle$ and σ are the mean and the standard deviation in the redshifts distribution calculated on the 485 galaxies considered in §5. Our catalogue C_{cen} is made of 320 galaxies, with redshifts between $cz = 5858$ km/s and $cz = 8168$ km/s.

| 1. structures | | | | | | 2. morphology | | | | | |
|---------------|-------|-----------|-----------|-----------|-------|---------------|-------|-----------|-----------|-----------|-------|
| scale | 99.9% | 3σ | 4σ | 5σ | voids | scale | 99.9% | 3σ | 4σ | 5σ | voids |
| 0.47 | 54 | 205 | 200 | 75 | 40 | 0.47 | 0.95 | 0.88 | 0.89 | 0.89 | 0.94 |
| 0.94 | 21 | 42 | 35 | 25 | 12 | 0.94 | 0.85 | 0.64 | 0.62 | 0.58 | 0.60 |
| 1.88 | 3 | 3 | 2 | 3 | 0 | 1.88 | 0.19 | 0.42 | 0.32 | 0.60 | - |
| 3.76 | 2 | 1 | 1 | 2 | 0 | 3.76 | 0.16 | 0.10 | 0.13 | 0.12 | - |

Table 4: Number of structures and mean morphological parameter $\langle L \rangle$ at different scales and over different thresholds for the catalog C . Scales are expressed in h^{-1} Mpc.

The mean redshift is $\langle cz \rangle = (7034 \pm 80)$ km/s and the standard deviation $\sigma_{cz} = (597 \pm 70)$ km/s. Our grid ensures a resolution of about $180 h^{-1}$ kpc on each of the three axis. We examine four different scales: 180, 360, 720 and $1440 h^{-1}$ kpc, for the usual values of the threshold ranging from 3σ to 5σ plus the 99.9% confidence level threshold, where σ is the standard deviation in the wavelet coefficient distribution for the selected scale. We show the wavelet coefficients distributions on the four scales in Fig.4. These are slightly asymmetric too, with the usual small queue towards the positive values, meaning presence of substructure also inside the central region of the cluster. Our results are expressed in terms of number of structures at the selected scales. Considering the 99.9% confidence level threshold as significance level for the structure detection, we have overwhelming evidence for substructure inside the central region of the Coma cluster on the first three scales investigated: 180, 360 and $720 h^{-1}$ kpc (see the Table 4A). The morphological parameter is shown in Table 4B. Our substructures are rather spherical on all the scales but the last one, with a value of about 0.5 of the morphological parameter, shows that the shape becomes more elongated on a scale of typical size $720 h^{-1}$ kpc inside the central region.

6.2. Search for segregation

Having identified the substructures we tried to search for any evidence of segregation, in luminosity and/or colour. Recently some evidence of morphological segregation within Coma has been found (Andreon, 1996). Unfortunately we had not enough morphological information to attempt an analysis of morphological segregation among the substructures we found. In fig. 6 we show that there is no evidence that the different subgroups observed within the central region of Coma differ as far as colour distribution $b - r$ is concerned. One must however keep in mind that this colour index is not strongly correlated with absolute b -magnitude, so that from this figure one cannot draw any conclusion about the presence of morphological segregation. We will examine these and other aspects of luminosity functions within Coma in a forthcoming paper.

7. Statistical Robustness and Physical Significance

Until now we have not tried to draw from this wavelet analysis of the combined angular-redshift distribution any conclusion about the real phase- and configuration-space structure of Coma. Before performing this further step one should verify that our catalogue does not suffer from any systematic selection biases or from other types of systematic effects like those induced by redshift distortions, as described by Regös & Geller (1989) and Praton & Schneider (1994). About these latter we notice that they have little significance for a cluster like Coma, because it lies at a distance of about $68 h^{-1}$ Mpc and from Table 5 we notice that the velocity dispersion of the structures found at a scale of $0.72 h^{-1}$ Mpc are at most of the order of 100 km/s, so the Hubble flow term is dominant over the peculiar velocity *within* these structures.

On one hand, one can reasonably argue that because the structures we find are well within the nonlinear virialized region on these scales we are probing a region of the phase

space detached from the Hubble flow, where the linearity between redshift and distance is completely lost. On the other hand one also expects that the phase-space distribution within the nonlinear region should be enough well-mixed within each clump (if there are any) that the substructures detected correspond to substructures in velocity space.

In order to check this latter hypothesis, following a suggestion of the anonymous referee, we have repeated the wavelet analysis on each of 20 realizations obtained by randomly “reshuffling” the original catalogue, i.e. redistributing randomly the redshifts among the galaxies while keeping the angular coordinates fixed. The results are reported in Tables 6-7, and are consistent with those found by Escalera & Mazure (1992) who performed a similar analysis for 2-D catalogues. The average values of the number of structures is always smaller than the one found in the original catalogue, showing that the catalogue itself is probably contaminated by some uncertainty, probably connected to the arbitrariness in the choice of the redshift limits, by some background contaminants, etc. However, notice for instance that at the scale $0.44 h^{-1}$ Mpc the number of structures found is 54 in the main catalogue, i.e. a value 3.13σ larger than the mean given by reshuffling over the galaxies in Table 7. This corresponds to a confidence level of 99.82%, i.e. a 0.18% probability of false detection. On the scale $720 h^{-1}$ kpc these figures become 99.33% for the confidence level and 0.67% for the probability of false detection. Interestingly enough, the mean value of structures found on this scale is 5, and a closer inspection reveals that the structures which do not disappear during the reshuffling are those numbered from 2 to 5 in Table 5.

This test strengthens our confidence on the physical significance of most of the structures detected, particularly when filtering on the scale of $720 h^{-1}$ kpc. Under this respect our results are consistent with those found by Escalera & Mazure (1992) on 2-D maps of simulated clusters, which demonstrated the ability of the wavelet analysis to recover substructures which are traced even by few objects. We will perform a more quantitative analysis of the statistical significance of our wavelet analysis of combined angular-redshift

catalogues in a forthcoming paper (Pagliaro et al., 1997a).

8. Conclusions and discussion

During the last years new redshift surveys and methods of analysis have allowed a more thorough understanding of structure of the Coma cluster (see e.g. Mellier et al., 1988; Escalera et al., 1992; CD96; Biviano et al., 1996), with most of the effort going to ascertain whether it can be classified as a relaxed one or not and to unveil hidden substructures. While this cluster has often in the past been modelled under the assumptions of homogenous velocity structure and spherical symmetry (see e.g. Kent & Gunn, 1982), the most recent observational evidence is pointing toward a more complex structure. The recent *ROSAT* images and 2-D optical analysis have strengthened the evidence for the existence of multiple substructure and suggest that Coma can not be considered a relaxed cluster. Under this respect, it is worth mentioning that already in 1988 Mellier et al. (1988), by analysing the isopleths within a 2-D map of the cluster had suggested the possible existence of 9 density peaks. In this paper, we have investigated the nature of the Coma cluster performing a 3-D analysis of the combined angular-redshift distribution of the cluster. We have assembled a catalogue of 798 galaxy redshifts, the largest presently available for the Coma cluster. Then, we have developed a 3-D wavelet and segmentation structure analysis that has allowed us to find out substructures on different scales and to describe them in a quantitative way. This powerful method of analysis has already provided excellent results in many fields of physics (e.g. Arneodo et al., 1988; Argoul et al., 1989; Slezak et al., 1990; Fujiwara & Soda, 1995; Grebenev et al., 1995).

Our results suggests that Coma can not be considered a regular cluster of galaxies, but it is filled up with substructure on all scales ranging from 720 kpc to $\sim 4 h^{-1}$ Mpc. The general diminution of the mean morphological parameter, meaning more elongated shapes,

and of the number of structures with the scale indicates a hierarchical distribution of the substructure.

We have examined the Coma cluster using three different subsamples of our catalogue (see Table 1); so we have insights within regions of different sizes with different resolutions.

On a scale of about $2 h^{-1}$ Mpc, our analysis on the extended Coma catalogue suggests the presence of multiple substructure with spherical morphology (see Table 2). On this scale a large number of voids is detected and their shapes are rather spherical. On the same catalogue, multiple substructure is still present at the scale $4 h^{-1}$ Mpc: on this scale shapes are more elongated ($\langle L \rangle = 0.67$). On scales $8 h^{-1}$ Mpc and $16 h^{-1}$ Mpc we find only two very elongated objects, in agreement with the histogram of Fig.1a. Voids on scales larger than $2 h^{-1}$ Mpc are few and very elongated. Although we cannot draw any conclusion before having made a comparison with N-body simulations (Pagliaro et al., 1997b), the presence of hierarchically organized substructure seems to point to an evolutionary scenario in which the Coma cluster and the galaxies included in the second peak of the histogram of the galaxy distribution in Fig. 1a were not generated by the collapse of two large spherical density perturbation with different masses and radius of about $15 h^{-1}$ Mpc, but by the merging of a large number of isolated spherical density perturbations of radius ranging from $1 h^{-1}$ Mpc to $3 h^{-1}$ Mpc. This first rough picture of the Coma evolution becomes more evident if we examine the catalogues C and C_{ext} .

Our analysis of the second catalogue (C) suggests the presence of substructures on all the scales with shapes becoming more elongated with growing scale (see Table 3) Voids are detected only on scales $0.47 \div 0.94 h^{-1}$ Mpc and their shapes are rather spherical ($0.60 \leq \langle L \rangle \leq 0.94$)

On smaller scales (hundreds of kpc) we have concentrated our analysis on a central region with redshifts $5858 \leq cz \leq 8168$ km/s. This region includes the core of Coma with

the galaxies NGC 4874 ($\langle cz \rangle = 7131$ km/s) and NGC 4839 ($\langle cz \rangle = 7397$ km/s). Multiple substructures are found on scales $180\div 720 h^{-1}$ kpc with rather spherical morphology ($0.50 \leq \langle L \rangle \leq 1.00$). A large number of spherical ($\langle L \rangle = 0.98$) voids is detected only on the smallest scale ($180 h^{-1}$ kpc). We stress however once again the fact that the interpretation of substructures on such small scales in terms of *real* substructures in velocity (or position) space is not as strong, as noted in the previous paragraph.

Finally, we concentrate on the scale of $720 h^{-1}$ kpc, where we have detected seven substructures that we show in Fig. 5 and which coincide with the peaks that we find in the central region of the histogram of Fig.1b. To each one of these object we can associate a dominant galaxy. Mean redshifts of the objects are: $cz \sim 5912$ km/s, $cz \sim 6100$ km/s, $cz \sim 6421$ km/s, $cz \sim 6775$ km/s, $cz \sim 7161$ km/s, $cz \sim 7594$ km/s and $cz \sim 7805$ km/s. In Table 5 we report some statistics only for the clumps containing a significant number of objects. To each clump singled out we can associate one or two dominant galaxies. These are (for increasing redshift): NGC 4934 & NGC 4840, NGC 4889, NGC 4898 & NGC 4864, NGC 4874 & NGC 4839, NGC 4927, NGC 4875. We then confirm the presence of the two subclusters already described by CD96, but in addition we have found statistical evidence for the existence of more substructures in redshift space. All this evidence leads us to suggest that the Coma cluster can not be considered a regular cluster of galaxies and that its process of formation occurs through a BOTTOM-UP mechanism as predicted by *CDM* and *MDM* models.

Finally, we would like to stress the fact that from this analysis it is difficult to draw any conclusion about the evolutionary state of this cluster. Such an analysis would require some modelling of the evolutionary scenarios through comparison with high-resolution N-body simulations and a better understanding of the velocity field around Coma. We will report on these issues in a subsequent work (Pagliaro et al., 1997b).

We would like to thank the anonymous referee for insightful comments which led to the introduction of the section on the statistical significance of the analysis performed in this paper. A.Pa. would like to thank E. Lega for having sent him her structure detection code, a copy of her Ph.D. dissertation and for kind and indispensable help during the period in which our code was developed and tested, and A. Bijaoui for a stimulating discussion held in Erice. M.Ga. wish to thank S. Shandarin for a clarifying discussion and helpful suggestions.

Structures at $720 h^{-1}$ kpc

| N. Clump | N. Gal. | cz_{min} | cz_{max} | $\langle cz \rangle$ | σ_{cz} | M_{vir} |
|----------|---------|------------|------------|----------------------|---------------|-----------|
| 1 | 18 | 7756 | 7866 | 7805 | 30 | 6.9 |
| 2 | 34 | 7510 | 7666 | 7594 | 39 | 16.8 |
| 3 | 71 | 6980 | 7350 | 7161 | 105 | 284 |
| 4 | 68 | 6572 | 6967 | 6775 | 102 | 286 |
| 5 | 22 | 6356 | 6491 | 6421 | 34 | 10.9 |
| 6 | 19 | 6028 | 6164 | 6100 | 36 | 12.4 |

Table 5: Substructures detected on the scale $720 h^{-1}$ kpc. Redshifts are in km/s. First column gives the number of the clump, the second the number of galaxies contained within the clump, the third the NGC number of the brightest galaxy, and the fourth the values of the masses are in unit of $10^{11} M_{\odot}$.

Statistical Tests on C_{cen}

| scale | $\langle n \rangle$ | σ_n | n_{min} | n_{max} |
|-------|---------------------|------------|-----------|-----------|
| 0.18 | 23.29 | 1.9 | 17 | 25 |
| 0.36 | 11.12 | 1.57 | 9 | 15 |
| 0.72 | 5.05 | 0.72 | 4 | 6 |
| 1.44 | 1.05 | 0.23 | 1 | 2 |

Table 6: Statistics on a number of “reshufflings” of redshifts in catalogue C_{cen} . In column 1 the scale in h^{-1} kpc is reported, columns 2-5 give the average, standard deviation, minimum and maximum number of structures found, respectively.

| Statistical Tests on \mathcal{C} | | | | |
|------------------------------------|---------------------|------------|-----------|-----------|
| scale | $\langle n \rangle$ | σ_n | n_{min} | n_{max} |
| 0.47 | 42.12 | 3.79 | 33 | 48 |
| 0.94 | 17.47 | 3.47 | 12 | 22 |
| 1.88 | 2.29 | 0.57 | 1 | 3 |
| 3.76 | 1 | 0 | 1 | 1 |

Table 7: Same as Table 6 for catalogue \mathcal{C} .

REFERENCES

- Abell, G.O., 1958, *ApJS*, 3, 211
- Andreon, S., 1996, *A&A*, 314, 763
- Argoul, F., Arneodo, A., Grasseau, G., Gagne, Y., Hopfinger, E.F. and Frisch, U., 1988, *Nature*, 338, 51
- Arneodo, A., Grasseau, G. and Holschneider, M., 1988, *Phys. Rev. Lett.*, 61, 2281
- Baier, F.W., Fritze, K., Tiersch, H., 1990, *Astron. Nachr.*, 311, 89
- Biviano, A., Durret, F., Gerbal, D., Le Fevre, O., Lobo, C., Mazure, A., and Slezak, E., 1996, *A&ASuppl. Ser.*, 111, 265
- Briel, U.G., Henry, J.P., Böhringer, H., 1992, *A&A*, 259, L31
- Colless, M., Dunn, A., M., 1996, *ApJ*, also astro-ph/9508070 (CD96)
- Escalera, E., and Mazure, A., 1992, *ApJ*, 388, 23
- Escalera, E., Slezak, E., Mazure, A., 1992, *A&A*, 264, 379
- Fitchett, M.J., Webster, R.L., 1987, *ApJ*, 317, 653
- Fujiwara, Y. & Soda, J., 1995, astro-ph/9509102
- Godwin, J., G., Metcalfe, N., Peach, J., V., 1983, *MNRAS*202, 113
- Grebenev, S.A., Forman, W, Jones, C. and Murray, S., 1995, *ApJ*, 445, 607
- Grossmann, A., Morlet, J., 1984, *SIAM J. Math.*, 15, 723
- Grossmann, A., Morlet, J., 1987, *Math. & Phys., Lectures on recent results*, ed. L.Streit, World Scientific

- Karachentsev, I., D., Kopylov, A., I., 1990, MNRAS, 243, 390
- Kent, S.M. and Gunn, J.E., 1982, AJ, 87, 945
- Lega, E., 1994, These de Doctorat, Université de Nice (L94)
- Lega, E., Bijaoui, A., Alimi, J.M., Scholl, H., 1996 ApJ, also astro-ph/9510156
- Lega, E., Scholl, H., Alimi, J.-M., Bijaoui, A., Bury, P., 1995, Parallel Computing, 21, 265
- Mazure, A., Proust, D., Mathez, G., Mellier, Y., 1988, A&A, 75, 339
- Mellier, Y., Mathez, G., Mazure, A., Chauvineau, B. and Proust, D., 1988, A&A, 199, 67
- Praton, E.A. and Schneider, S.E., 1994, ApJ, 422, 46
- Pagliari, A. and Becciani, 1997, A parallel code for structure detection (in preparation)
- Pagliari, A., Antonuccio-Delogu, V., Becciani, U., Gambera, M., 1997a, (in preparation)
- Pagliari, A., Antonuccio-Delogu, V., Becciani, U., Gambera, M., 1997b, (in preparation)
- Regös, E. and Geller, M.J., AJ, 98, 755
- Rosenfeld, A., 1969, Picture Processing by Computer, Academic Press, New York
- Slezak, E., Bijaoui, A., Mars, G., 1990, A&A, 227, 301
- White, S.D.M., Briel, U.G., Henry, J.P., 1993, MNRAS, 261, L8
- Zwicky, F., 1933, Helv.Phys.Acta 6, 10

Fig. 1.— (a) Histogram of the galaxy distribution, with redshifts $3000 \leq cz \leq 28000$ km/s inside C_{ext} , according to our catalogue. Step is 500 km/s; (b) histogram of the galaxy distribution, with redshift $4000 \leq cz \leq 10000$ inside C , according to our catalogue. Step is 100 km/s.

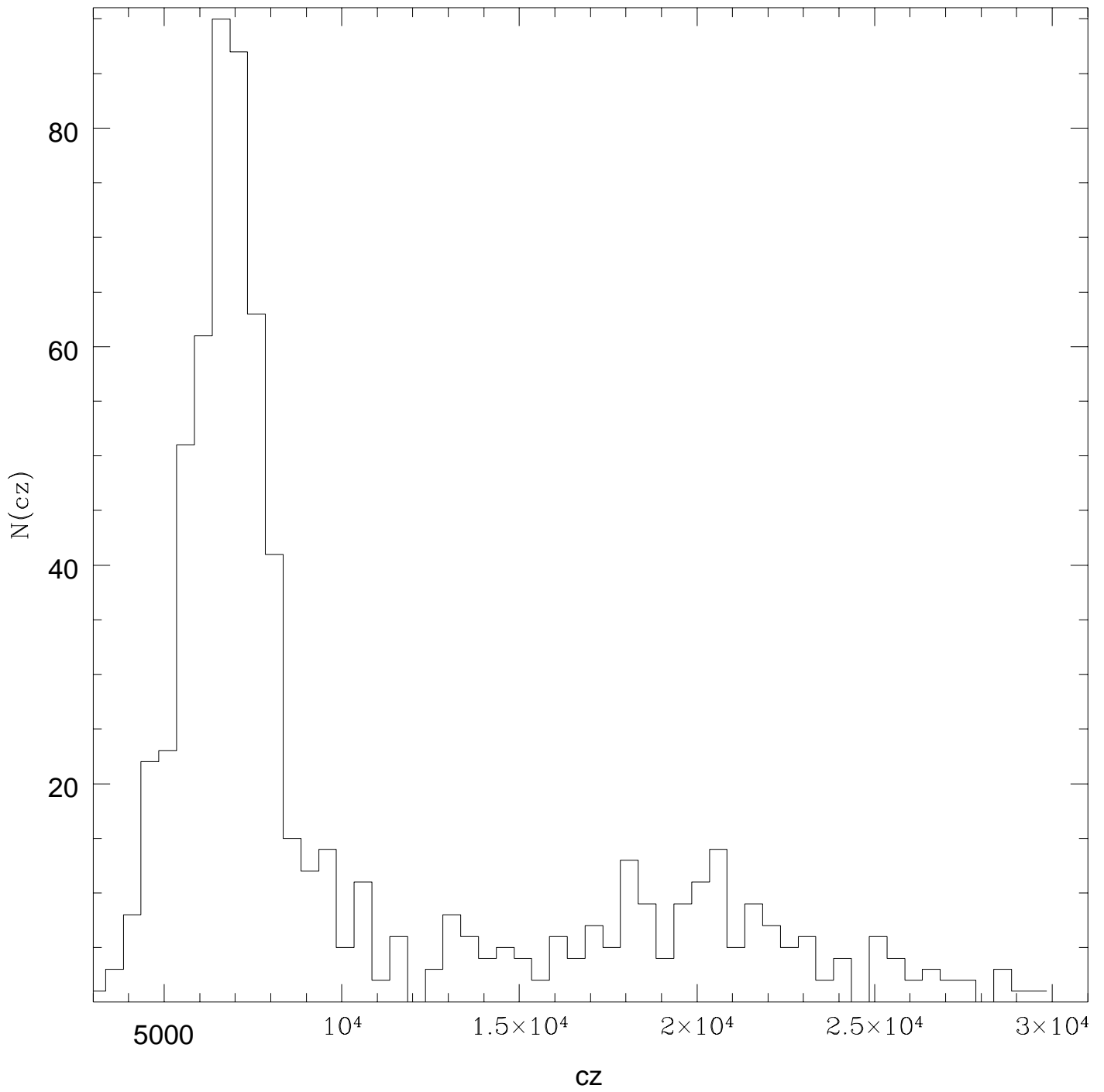
Fig. 2.— Histograms of the wavelet coefficients on the four scales selected for C_{ext}

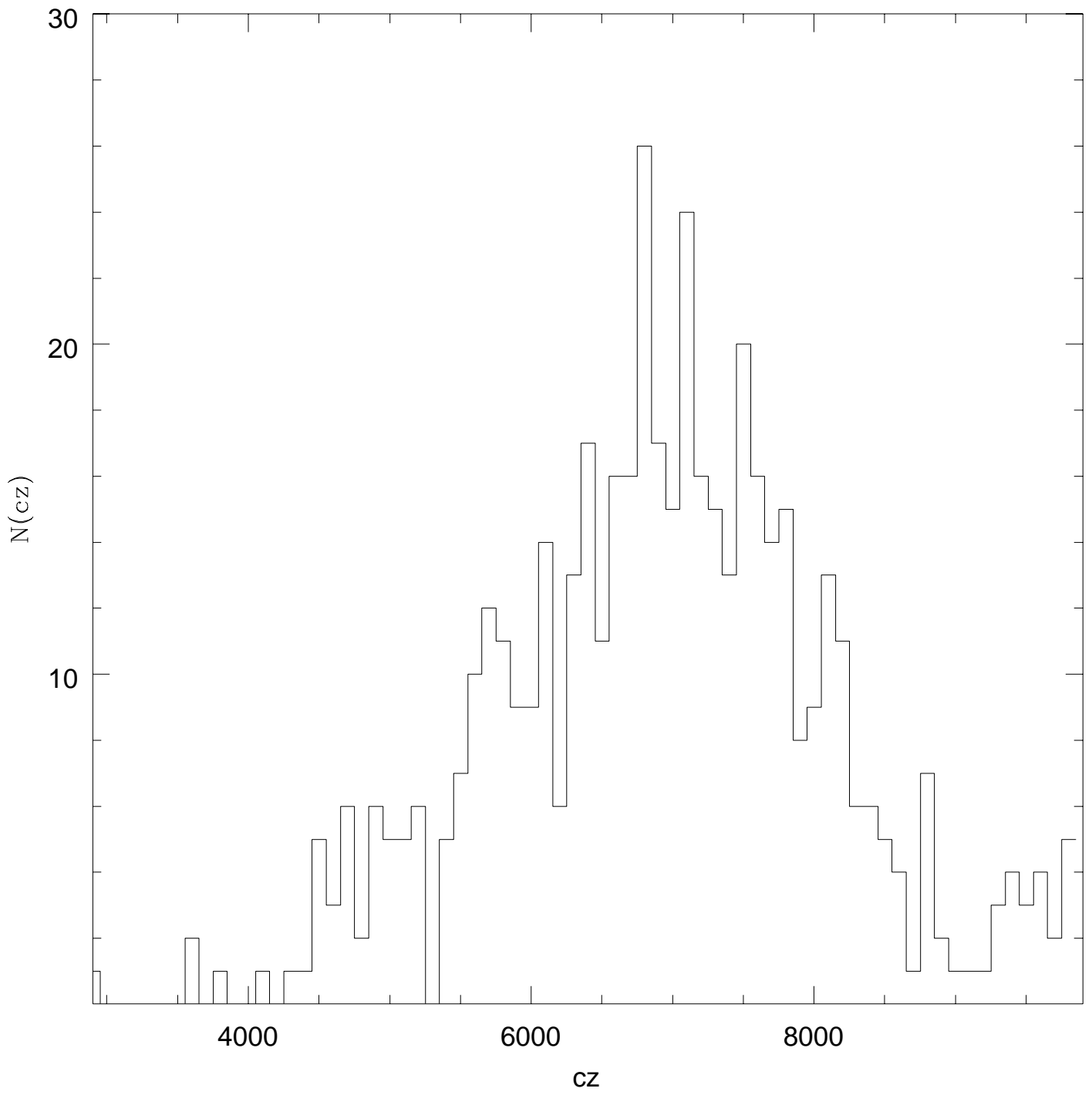
Fig. 3.— Histograms of the wavelet coefficients on the four scales selected for C

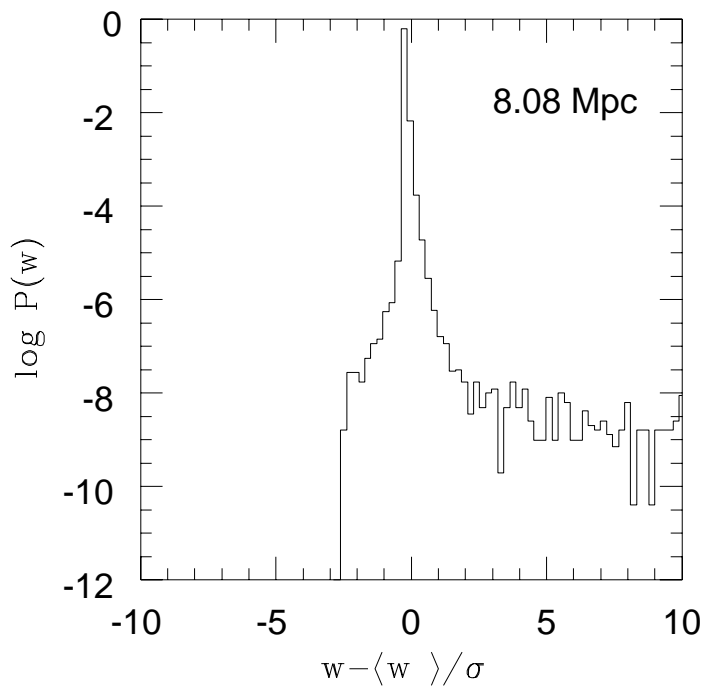
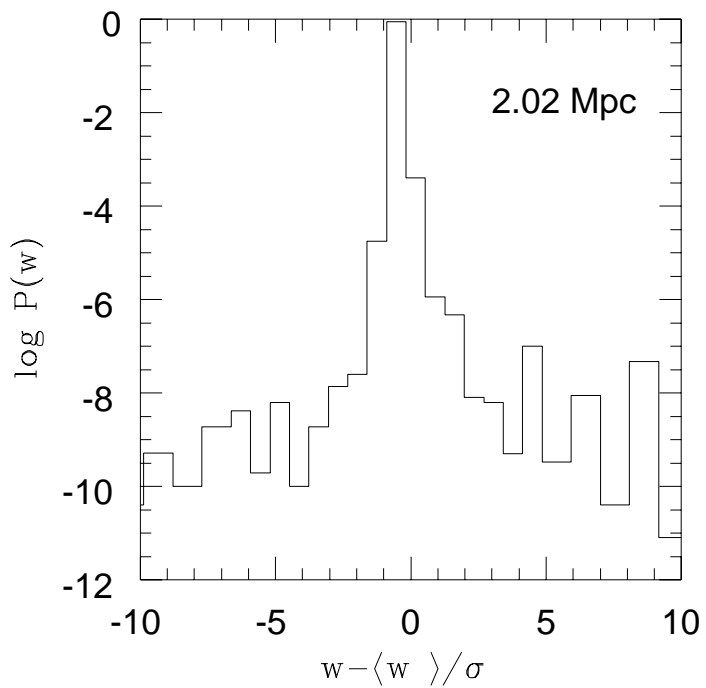
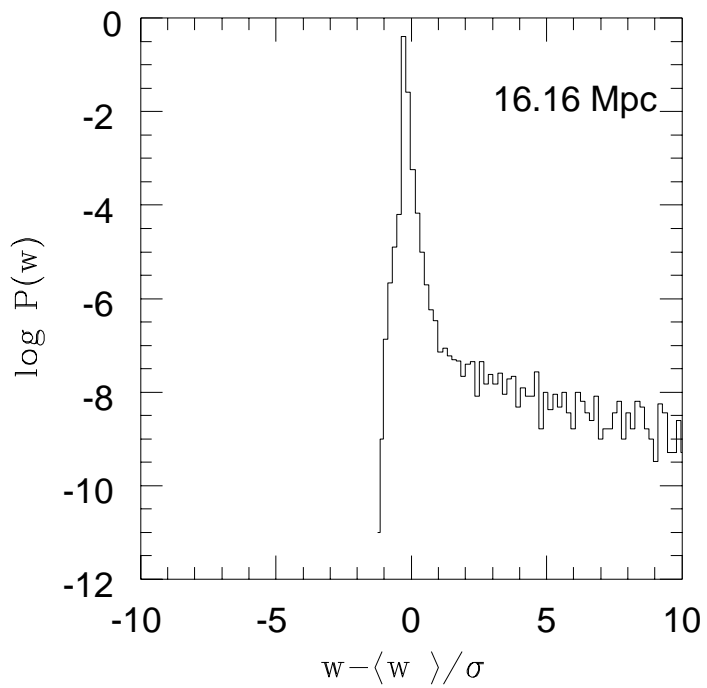
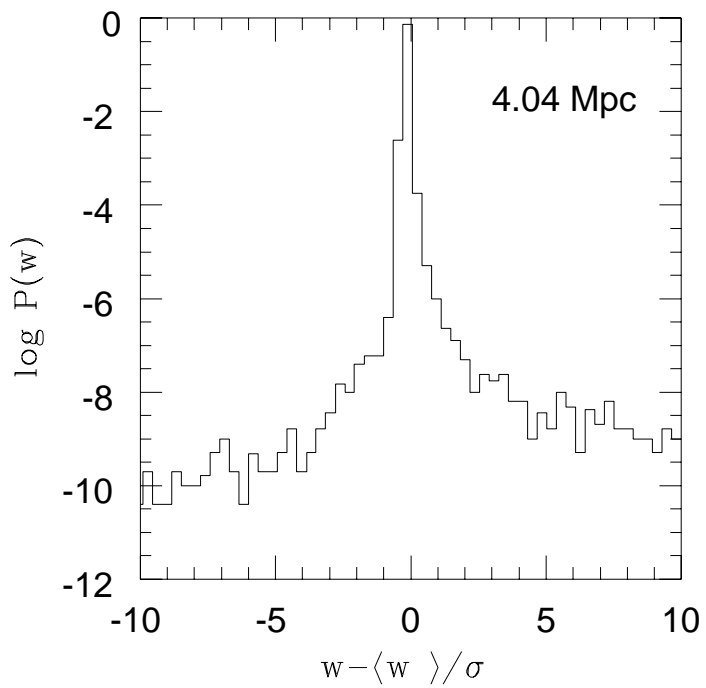
Fig. 4.— Histograms of the wavelet coefficients on the four scales selected for C_{cen}

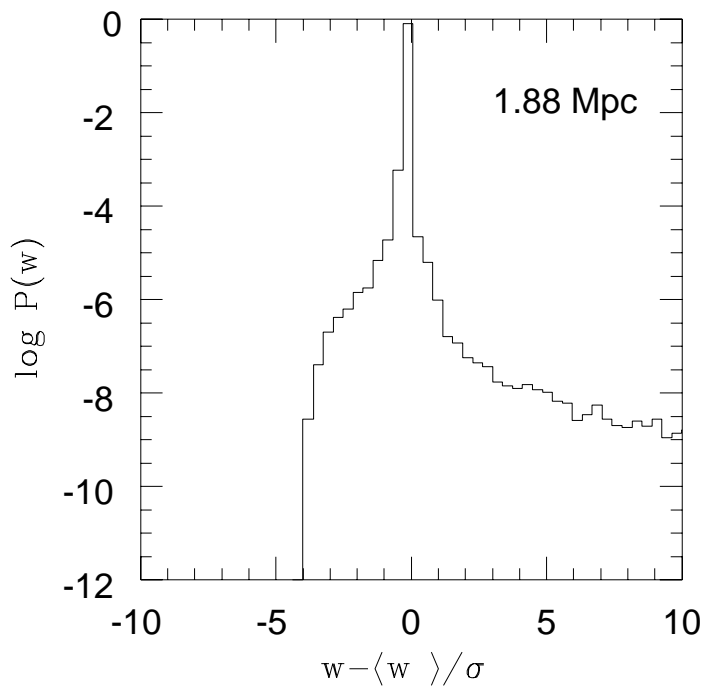
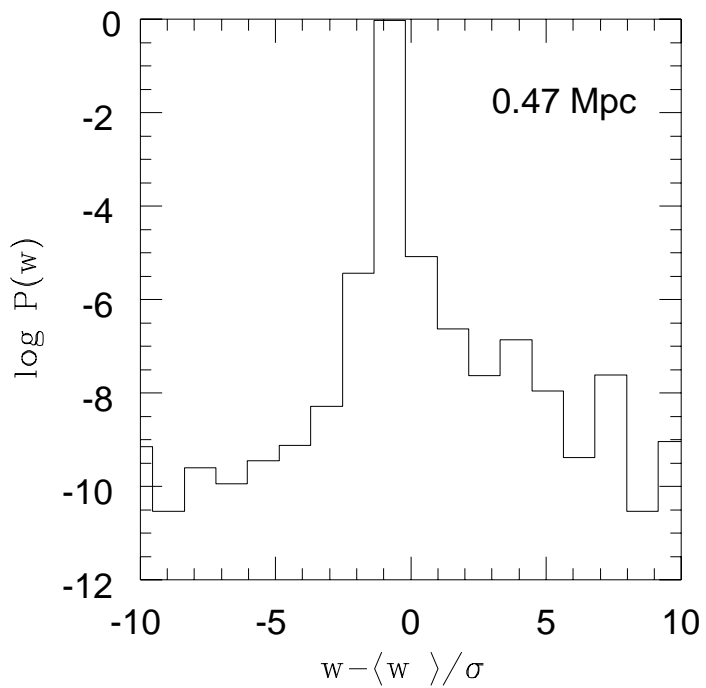
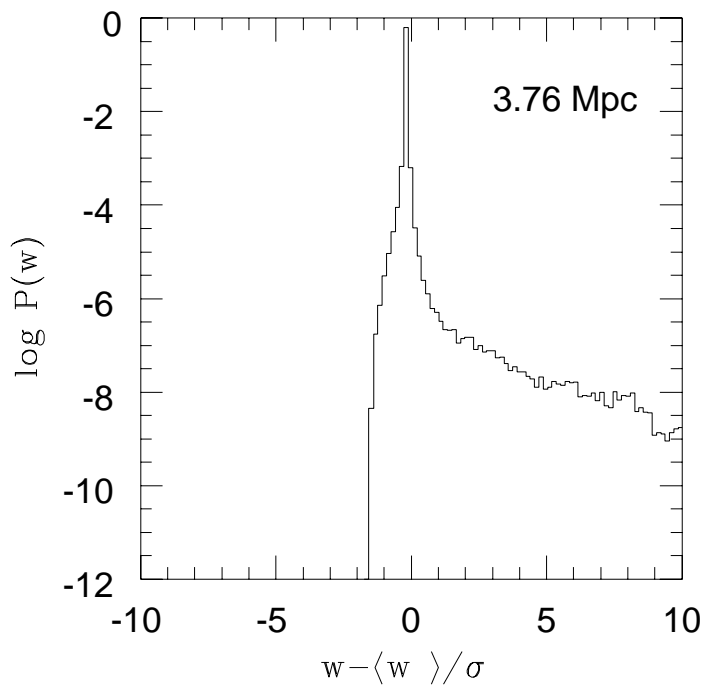
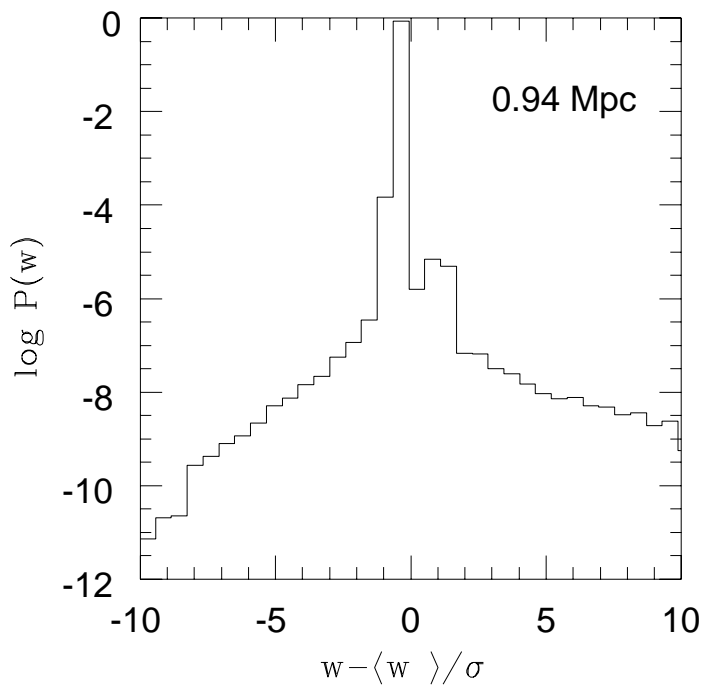
Fig. 5.— Substructures for the central region of Coma detected with a resolution of $720 h^{-1}$ kpc. The seven structures detected are clearly visible. Morphological parameter: $\langle L \rangle = 0.50$

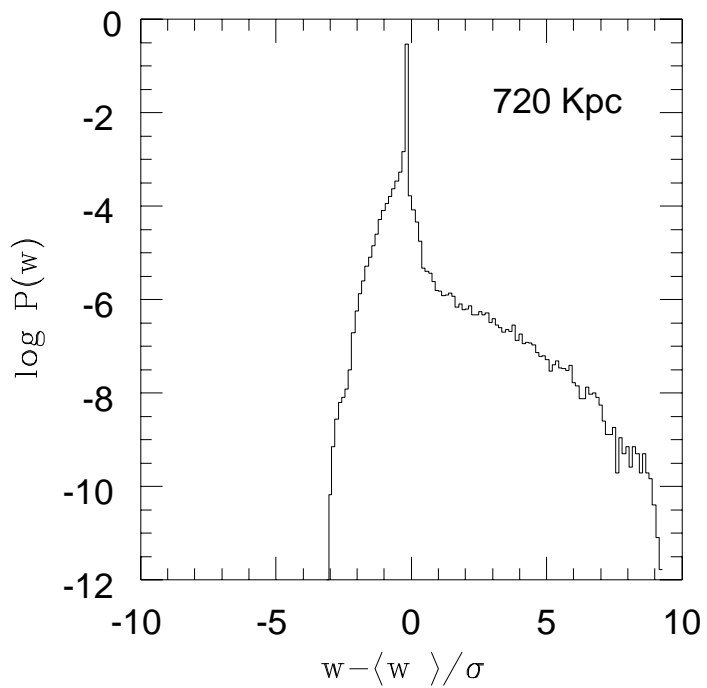
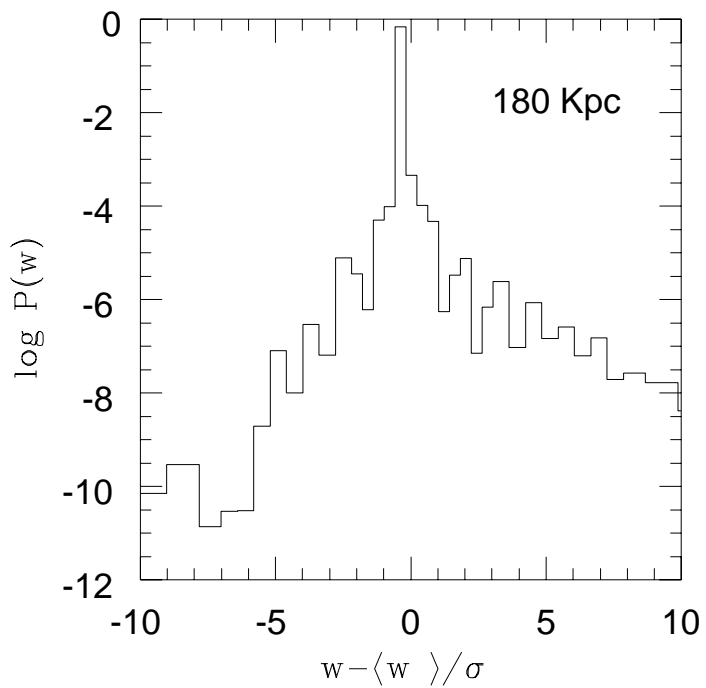
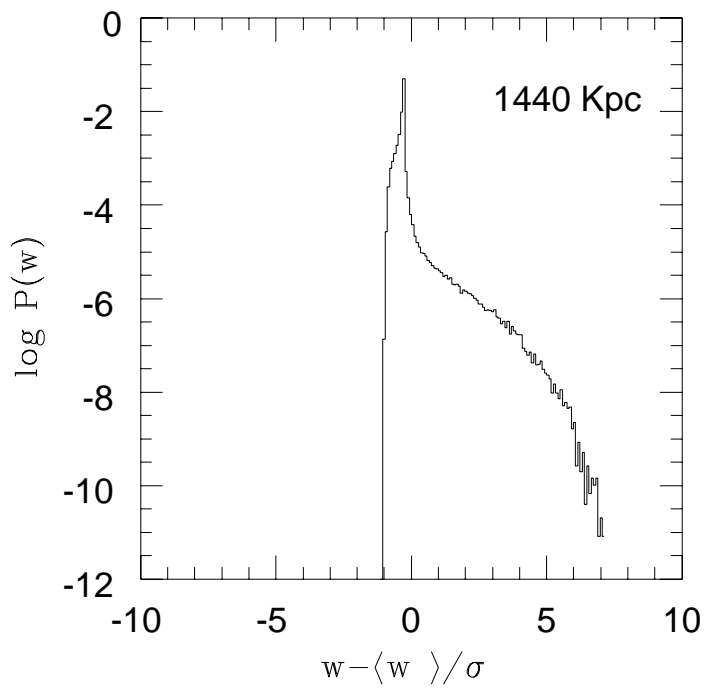
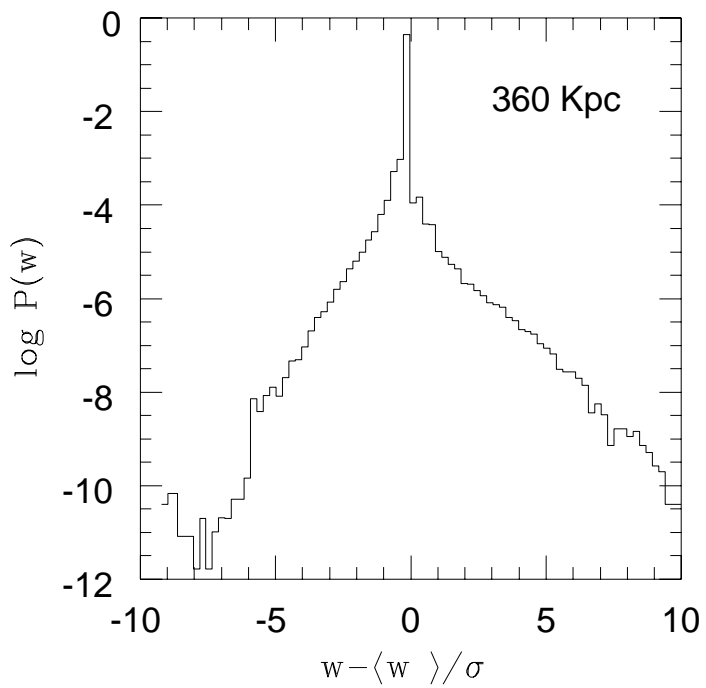
Fig. 6.— Colour segregation. The different histograms refer to the substructures of Table 5, and are numbered according to the first column of that table.











COMA
CENTRAL
REGION

